Arabidopsis GRI is involved in the regulation of cell death induced by extracellular ROS

Michael Wrzaczek[a], Mikael Brosché[a], Hannes Kollist[a,b], and Jaakko Kangasjärvi[a,1]

[a]Plant Biology, Department of Biological and Environmental Sciences, University of Helsinki, P.O.B. 65, FI-00014 Helsinki, Finland; and [b]Institute of Technology, University of Tartu, EE-50411 Tartu, Estonia

Reactive oxygen species (ROS) have important functions in plant stress responses and development. In plants, ozone and pathogen infection induce an extracellular oxidative burst that is involved in the regulation of cell death. However, very little is known about how plants can perceive ROS and regulate the initiation and the containment of cell death. We have identified an *Arabidopsis thaliana* protein, GRIM REAPER (GRI), that is involved in the regulation of cell death induced by extracellular ROS. Plants with an insertion in *GRI* display an ozone-sensitive phenotype. *GRI* is an *Arabidopsis* ortholog of the tobacco flower-specific *Stig1* gene. The GRI protein appears to be processed in leaves with a release of an N-terminal fragment of the protein. Infiltration of the N-terminal fragment of the GRI protein into leaves caused cell death in a superoxide- and salicylic acid-dependent manner. Analysis of the extracellular GRI protein yields information on how plants can initiate ROS-induced cell death during stress response and development.

superoxide | STIG1 | salicylic acid

Reactive oxygen species (ROS) have earlier been considered merely as cytotoxic compounds, but clearly, their functions are far more diverse. They have important and tightly regulated roles as signaling molecules in disease resistance, stress adaptation, and development in many organisms (1, 2). In plants, ROS are produced in response to many stresses, including pathogen attack, osmotic stress, excess light, wounding, and ozone (O_3), in different subcellular compartments (1). For example, pathogen attack and O_3 induce an oxidative burst in the extracellular space, whereas high light or the herbicide methyl viologen lead to the production of ROS in the chloroplast (1). ROS also serve as second messengers in abscisic acid (ABA) signaling in the regulation of the stomatal aperture (3) and are involved in root hair growth (4). In angiosperm flowers, ROS are present in pollen and stigmas (5) and regulate pollen tube growth (6), but they might also have further functions including self-incompatibility and pathogen defense (5).

Cells decipher ROS signals with regard to type, localization, and timing of ROS produced (7), but mechanisms of ROS perception have remained mostly obscure. Only a few examples have linked the cellular machinery to perception and integration of ROS signals. Plant heat-shock transcription factors (HSFs) might function as H_2O_2 sensors (8), and the salicylic acid (SA) signaling protein NPR1 confers redox regulation to the transcription factor TGA1 (9). Various components of the ROS detoxification machinery could be used to detect differences in the oxidative load (9, 10). However, the mechanisms and processes involved in the ROS perception and signaling in the extracellular space have remained almost completely elusive.

Programmed cell death (PCD) is a common response to various environmental and developmental cues (7). In plant–pathogen interactions, the hypersensitive response (HR) protects plants against a biotrophic pathogen by isolating it in a patch of dead tissue. Limitation of cell death is crucial because extended tissue loss would have detrimental effects. In extreme cases, the inability to regulate lesion spread can lead to the death

of the plant (7, 11, 12). ROS are centrally involved in the regulation of PCD (7), but the precise roles in lesion initiation, spread, and containment are not well characterized. Potentially, ROS can function as both positive and negative regulators of PCD, depending on conditions and requirements (7, 12, 13).

In this study, we characterize a component involved in the regulation of stress-induced cell death in plants. The GRIM REAPER (GRI) protein is an *Arabidopsis* ortholog of the tobacco stigma-specific protein 1 (STIG1) (14). STIG1 helps to regulate exudate secretion in the pistils of petunia and tobacco (15). Tomato LeSTIG1 binds to the extracellular domain of pollen receptor kinases and promotes pollen tube growth in vitro (16). However, no roles for STIG1 have been described in vegetative tissues or in the regulation of cell death. Here, we present evidence that GRI is involved in the regulation of ROS-induced cell death in *Arabidopsis* leaves in a superoxide- and SA-dependent manner.

Results

Isolation and Identification of an Ozone-Sensitive *Arabidopsis thaliana* Mutant. A reverse genetic screen for ozone sensitivity was performed in *Arabidopsis* with ≈80 T-DNA and transposon lines bearing insertions in O_3-regulated genes [supporting information (SI) Table S1]. Plants were exposed to 300 parts per billion (ppb) O_3 for 6 h. One O_3-sensitive line was a dSPM insertion mutant (SM_3.39219) in the locus At1g53130; leaves of the O_3-exposed plants exhibited HR-like lesions of collapsed tissue (Fig. 1*A*). The mutant was designated *grim reaper* (*gri*). Cell death, quantified as ion leakage, was significantly increased in *gri* when compared with clean-air controls and O_3-exposed wild-type Col-0 plants (Fig. 1*B*). Plant O_3-sensitivity can be a result of altered stomatal function with increased O_3 entry to the leaves (3). In *gri*, stomatal regulation was not impaired (Fig. S1*A*), and O_3 uptake to the leaf was the same as in Col-0 (Fig. S1*B*), suggesting that O_3 sensitivity of *gri* is caused by impaired sensing of, or response to, O_3 or ROS derived from O_3 by mesophyll cells.

***GRI* Encodes a Small Protein with Predicted Extracellular Localization.** The intronless *GRI* gene encodes a 18.6-kDa protein of 169 aa with a STIG1 domain (PF04885, amino acids 33–168) and a predicted N-terminal signal peptide (amino acids 1–30) for the secretory pathway (Fig. S2*A*). The STIG1 domain indicates that GRI is related to tobacco and petunia stigma-specific protein, STIG1 (14, 15). The tobacco *Stig1* encodes a small secreted protein present in the stigmatic lipid exudates. In *Arabidopsis*, *GRI* belongs to a small gene family of 6 members (Fig. S2*B*).
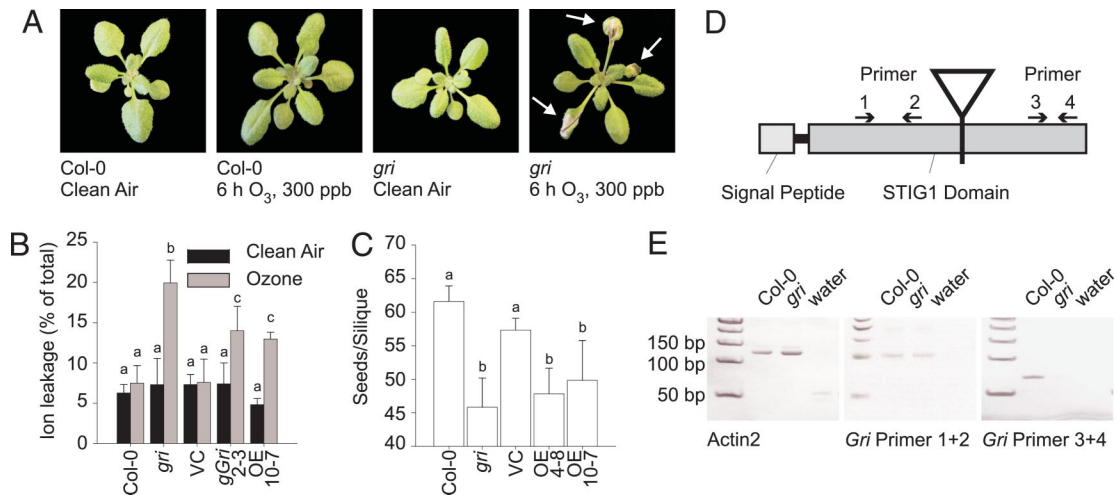
Fig. 1. *gri* plants show increased ROS-induced cell death and reduced seed content. (*A*) Col-0 and *gri* plants were exposed to 300 ppb O_3 for 6 h. *gri* plants showed lesions after O_3 treatment, whereas no damage was visible in Col-0. (*B*) Ion leakage was determined 8 h after the onset of O_3 exposure. In *gri*, but not in Col-0 and vector control (VC), ion leakage increased after exposure to O_3. In *gri* plants carrying a genomic complementation construct (*gGri*) and plants overexpressing GRI-c-myc (OE), ion leakage increased after O_3 treatment compared with Col-0, however, to lesser levels than in *gri*. The experiment was repeated 5 times with similar results. Four genomic complementation and overexpression lines were tested, and representative results from 1 line are shown. (*C*) The seed content in siliques was reduced in *gri* and GRI overexpressors compared with Col-0 and vector control. (*D*) GRI protein possesses a signal peptide and a STIG1-domain. The dSPM insertion site in *gri* and the location of primers used for RT-PCR experiments are shown. (*E*) RT-PCR analysis showed that the full-length *GRI* transcript was absent from *gri* plants. Primers 1 and 2 show the transcript before the insertion in Col-0 and *gri*. Primers 3 and 4 show a transcript in Col-0 but not in *gri* after the insertion site. Actin-2 transcript is present in Col-0 and *gri* plants. In *B* and *C*, all data points are mean ± SD (in *B*, n = 4; in *C*, n = 6). Bars labeled with a different letter differ significantly ($P < 0.05$) by Tukey's honestly significant difference (HSD) test.

Neighbor-joining and distance analyses point to GRI as the *Arabidopsis* ortholog of tobacco STIG1 (Fig. S2 *B* and *C*).

GRI Expression Is Very Low in Leaves and High in Flowers. The *GRI* transcript was present in leaves at very low levels and showed a slight circadian variation in its expression (Table S2). In flowers, *GRI* expression was 1,000-fold higher than in leaves. Despite the very low expression of *GRI* in leaves, a clear O_3-sensitive leaf phenotype was visible in *gri* (Fig. 1*A*) and exposure to 300 ppb O_3 for 6 h increased *GRI* transcript abundance in leaves ≈2- to 3-fold.

Seed Content Is Reduced in *gri* Siliques. The only phenotype observed after silencing of tobacco *Stig1* was an acceleration of secretion of the stigmatic exudate and a slightly different appearance of the stigma (15). In *gri*, no apparent changes of flower morphology were found, but the seed content of the siliques was reduced in *gri* and GRI-c-myc/StrepII overxpression plants compared with Col-0 (Fig. 1*C*).

Infiltration of *Arabidopsis* Leaves with GRI-Peptide Induces Cell Death. In genetic complementation assays, the O_3-sensitive phenotype of *gri* was not fully complemented when *gri* plants were transformed with the genomic clone of *GRI* (Fig. 1*B*). In addition, Col-0 plants overexpressing the *GRI* ORF with a C-terminal c-myc/StrepII tag under the control of the cauliflower mosaic virus 35S promoter showed a similar O_3-sensitive phenotype as *gri*. Ion leakage after O_3 treatment was not as strongly increased in the complementation and overexpression lines as in the *gri* mutant, but the levels were clearly increased compared with Col-0 (Fig. 1*B*). The location of the dSPM insertion in *gri* (Fig. 1*D*) suggested that a N-terminal part of the GRI protein (96 aa including the signal sequence) might still be produced in the *gri* mutant. Indeed, RT-PCR analysis indicated that *GRI* transcript abundance was similar in Col-0 and *gri* upstream of the insertion site, whereas downstream of the transposon insertion, the *GRI* transcript was not detectable by PCR in *gri* (Fig. 1*E*). This implied that *gri* plants could express a truncated GRI protein

that could cause the observed phenotypes. Alternatively, the observed phenotypes might be due to partial cosuppression of the *GRI* gene.

When the GRI protein with C-terminal c-myc/StrepII tag was expressed in Col-0, in addition to the ≈35-kDa GRI-c-myc/StrepII fusion protein, a smaller, ≈25-kDa protein was recognized by the α-c-myc antibody (Fig. 2*A*). This implies that an ≈10-kDa fragment is released from the N terminus of the fusion protein. Because of the predicted size of the GRI signal peptide (30 aa, ≈3.5 kDa), the released N-terminal fragment would contain ≈60–70 additional amino acids of the GRI protein. A peptide predicted to be present in the *gri* mutant, corresponding to amino acids 31–96 after the signal peptide sequence (GRI-peptide), was targeted for further study.

GRI-peptide was produced in *Escherichia coli* and purified by using a GST tag. The recombinant protein was infiltrated into Col-0 leaves, and cell death was quantified as ion leakage. Infiltration with the GST-GRI-peptide or the GRI-peptide without the GST-tag induced ion leakage, whereas bacterially produced GST or buffer alone had no such effect (Fig. 2*B*). This offers an explanation for the incomplete rescue of the *gri* mutant by genomic complementation and also for the O_3-sensitive phenotype of the plants overexpressing the GRI-c-myc/StrepII fusion protein. The presence of a truncated protein in *gri* plants, corresponding to GRI-peptide, can cause cell death under conditions of extracellular oxidative stress, which is apparent as increased sensitivity to O_3.

GRI-Peptide-Induced Cell Death Is Superoxide Dependent. Cell death was increased in *gri* plants only under stress conditions. To test whether ROS were required for the induction of cell death, we included ROS scavengers in the infiltration buffer together with GRI-peptide. The removal of superoxide through coinfiltration with superoxide dismutase (SOD) reduced GRI peptide-induced cell death to control levels (Fig. 2*C*). Catalase (CAT), a H_2O_2 scavenger, also slightly reduced ion leakage. GRI-peptide did not cause increased cell death in *atrbohD*, a mutant in the plant respiratory burst NADPH oxidase generating su-
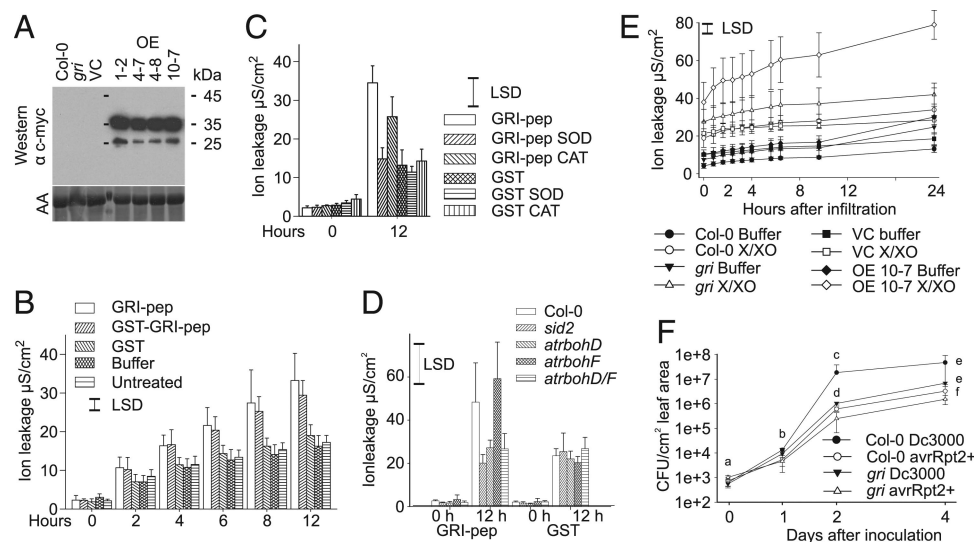
Fig. 2. A short GRI peptide is capable of inducing cell death in a superoxide-dependent manner. (*A*) GRI-c-myc/StrepII protein is present in plants overexpressing GRI. Western blot analysis with α-c-myc antibody detects a 35- and 26-kDa GRI-C-terminal c-myc/StrepII fusion protein. Both proteins are absent in Col-0, *gri*, and vector control (VC). Equal loading was shown by amido black staining. (*B*) Infiltration of GRI-peptide into Col-0 leaves induced cell death. (*C*) Coinfiltration of GRI-peptide with SOD and CAT reduced cell death. (*D*) Cell death induction by GRI-peptide is reduced in *atrbohD*, *atrbohD/F*, and *sid2*. However, in *atrbohF*, cell death is induced similarly to Col-0. (*E*) X/XO infiltration into leaves induced more cell death in *gri* and OE plants than in Col-0. In *B–E* data points are mean ± SD (*n* = 6), differences larger than LSD shown are statistically significant (*P* < 0.05) by the modified least-significant difference test. (*F*) Growth of virulent *Pst* DC3000 was reduced in *gri* compared with WT, whereas the growth of an avirulent variant (*Pst* DC3000 avrRpt2+) was not affected. Data points are mean ± SD (*n* = 3). Bars labeled with different letters differ significantly (*P* < 0.05) by Tukey's HSD test.

peroxide, but in *atrbohF*, cell death was induced to a similarly to Col-0 (Fig. 2*D*). Induction of cell death in *atrbohD/F* was similar as in *atrbohD*. GRI-peptide was not able to induce cell death in *sid2*, impaired in SA biosynthesis, whereas a weaker reduction in the level of GRI-peptide-induced cell death was observed in *triple fad*, impaired in jasmonic acid (JA) biosynthesis, and in *ein2*, impaired in ethylene signaling (Fig. S3). Infiltration of leaves with the exogenous superoxide producing system xanthine and xanthine oxidase (X/XO), which enzymatically generates superoxide in the extracellular space (14), caused increased cell death in the *gri* mutant (Fig. 2*E*). The *gri* plants also accumulated substantial amounts of superoxide after exposure to O_3 (Fig. S4). These results together demonstrate that the cell death-inducing effect of GRI-peptide depends on the presence of superoxide and SA.

***gri* Is More Resistant to a Virulent Bacterial Pathogen.** O_3-induced cell death shares similarities with the pathogen-induced HR (1, 7). Both events feature an extracellular oxidative burst, which is involved in the regulation of hypersensitive cell death and other defense pathways (1). Thus, altered sensitivity to ROS in cell death initiation in *gri* could have an impact on plant resistance to pathogens. We addressed this in growth assays with the virulent pathogen *Pseudomonas syringae pv*. tomato DC3000 (*Pst*) and avirulent DC3000 *avrRpt2+*. *gri* plants showed increased resistance to the virulent strain, but no change in the growth of the avirulent strain (Fig. 2*F*). Cell death progressed at a faster rate in response to both virulent and avirulent strains in the *gri* mutant compared with control plants (Fig. S5). Taken together, these results suggest that increased cell death in *gri* might lead to the increased resistance to a virulent bacterial pathogen and faster induction of cell death to avirulent pathogens.

Hormone Responses Are Suppressed in the *gri* Mutant. Several hormones are involved in plant stress responses, notably SA, JA, and ethylene (7). To investigate whether signaling pathways involving these 3 hormones were disturbed in *gri,* we analyzed

the expression of marker genes for these hormones (Table 1). Upon O_3 exposure *ICS1*, encoding a protein required for SA biosynthesis, was induced strongly in Col-0, but weakly in *gri*. The induction of downstream SA target genes, *PR1* and a putative ABC transporter At1g15520, was similarly reduced in *gri*. JA marker genes *LOX4* and *MDHAR* (monodehydroascorbate reductase) were induced by O_3 in Col-0, but in *gri* this induction was mostly absent. Another JA defense marker, *PDF1.2*, showed an earlier induction in *gri* compared with Col-0, but at later time points the transcript did not accumulate to the same levels as in Col-0. The induction of *ACS6*, encoding the rate-limiting enzyme in O_3-induced ethylene biosynthesis, was not altered in *gri* after O_3 exposure when compared with Col-0. In summary, this shows that responses leading to the initiation of SA- and JA-related processes are disturbed in *gri*, whereas ethylene-related processes remain unaffected.

Altered marker gene expression could be a result of altered hormone accumulation; thus, we analyzed hormone concentrations after O_3 exposure (Fig. 3). Concentrations of free SA and JA under control conditions were not significantly different between Col-0 and *gri*. No induction of SA and JA was observed at 2 h after the onset of O_3 treatment. However, free SA and JA accumulated to lower levels in *gri* than Col-0 8 h after onset of the O_3 treatment. The concentration of ABA, another plant hormone implicated in the responses to various stresses (17) did not differ between Col-0 and *gri* after O_3 exposure (Fig. S6). These results indicated that SA and JA accumulation, typical for O_3-induced cell death, was strongly reduced in *gri*.

GRI Protein Is Secreted to the Extracellular Space. The presence of an N-terminal signal peptide for secretion indicates that the GRI protein could be secreted to the extracellular space. To test this, the GRI protein-coding sequence (amino acids 1–169) was fused in-frame with yellow fluorescent protein (YFP). In addition, the GRI-coding sequence lacking the N-terminal signal peptide (amino acids 31–169) and the GRI signal peptide alone (amino acids 1–30) were fused with YFP. Onion epidermal cells were transiently transformed with the constructs via particle bom-

Table 1. Hormone signaling is impaired in *gri*

	Fold difference					
	2 h		8 h		24 h	
Marker gene	Col-0	*gri*	Col-0	*gri*	Col-0	*gri*
ICS1	2.7	1.9[A]	6.3[B]	4.6[C]	1.9[A]	1.2[D]
PR1	0.6[A]	2.4[C]	10.9[B]	1.0[A]	2.0[C]	1.3[A]
ABC tr.	11.3[A]	4.4[C]	25.3	11.9[A]	1.3[B]	1.4[BC]
LOX4	0.2[A]	0.4[AC]	5.7	1.2[BC]	0.9[AB]	0.7[A]
MDHAR	1.6[AC]	0.9[C]	4.6[B]	2.0[A]	0.9[C]	0.7[C]
PDF1.2	1.2	15.3[A]	36.2[B]	19.1[A]	42.8[C]	24.3[A]
ACS6	3.9[A]	1.3[C]	4.6[AB]	5.8[B]	1.0[C]	1.1[C]

Expression of marker genes for hormone signaling was analyzed by quantitative real-time RT-PCR. The expression of SA biosynthesis and signaling marker genes [*ICS1*, *PR1*, *ABC transporter* (*tr.*)] was reduced in *gri* compared with Col-0 as well as markers for JA signaling (*LOX4*, *MDHAR*, *PDF1.2*). Transcriptional induction of *ACS6*, a marker for ethylene biosynthesis, was not impaired in *gri* compared with Col-0. Shown are representative results from 1 of 5 experiments. Data points are mean ($n = 3$). Data points labeled with a different letter (superscript letters) differ significantly ($P < 0.05$) by Tukey's HSD test.

bardment and the subcellular localization of the protein-YFP fusions was examined by confocal microscopy (Fig. 4). YFP alone (Fig. 4 *A–D*) and GRI (31–169)-YFP (Fig. S7 *E–H*) missing the N-terminal signal localized to cytoplasm and nucleus. After plasmolysis, fluorescence was visible only in cytoplasm detached from the cell wall and in the nucleus. In cells expressing GRI (1–30)-YFP and GRI (1–169)-YFP, the fusion protein was detected in the cytoplasm. However, in plasmolyzed cells, the fusion protein was also visible in the extracellular space in regions where the plasma membrane detached from the cell wall (Fig. 4 *E–H* and Fig. S7 *A–D*, indicated with arrows). Under similar conditions the SLAC1-YFP fusion protein, which localizes to the plasma membrane (3), did not display any signal from the cell wall (Fig. S7 *I–K*). Taken together, the results indicate that GRI (1–169)-YFP and GRI (1–30)-YFP fusion proteins were secreted to the extracellular space.

Discussion

Here, we present evidence for the involvement of *Arabidopsis* GRIM REAPER (GRI) protein in the positive regulation of ROS-induced cell death. The GRI protein is related to tobacco STIG1, which is predominantly present in tobacco stigma and required for stigmatic lipid exudate secretion (15). The tomato ortholog, LeSTIG1, binds the extracellular domain of 2 pollen receptor kinases in vitro (16). Consistent with a role for STIG1

in flowers, *GRI* transcript abundance is very low in *Arabidopsis* leaves and significantly higher in flowers (Table S2). Unlike tobacco, *Arabidopsis* stigma do not secrete lipid exudates, which makes comparisons between tobacco STIG1-antisense plants and *gri* difficult. However, whereas *gri* flowers looked normal, the seed content in *gri* siliques was reduced. Furthermore, *gri* crosses had severely reduced efficiency, supported by the reduction of the seed number of siliques (Fig. 1*C*), suggesting that GRI also has a function in *Arabidopsis* flowers.

A function for STIG1 has been shown in tobacco and petunia flowers, but no connection to vegetative tissues or cell death has been implicated. The O_3-sensitive phenotype of the *Arabidopsis gri* mutant, hallmarked by lesion development and increased ion leakage after O_3 exposure, demonstrates important cell death- and ROS-related functions of GRI in vegetative tissues. The O_3-sensitive phenotype of the GRI-overexpression plants (Fig.
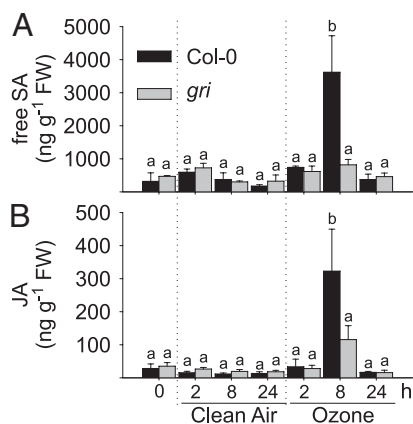
Fig. 3. Salicylic acid and jasmonic acid induction is reduced in *gri*. Plants were exposed to 300 ppb O_3 for 6 h. Samples were taken at 0, 2, 8, and 24 h after onset of ozone exposure from exposed and clean air control plants. The concentrations of plant hormones free salicylic acid (SA) (*A*) and jasmonic acid (JA) (*B*) were measured. Data points are mean ± SD ($n = 3$). Bars labeled with different letters differ significantly ($P < 0.05$) by Tukey's HSD test.
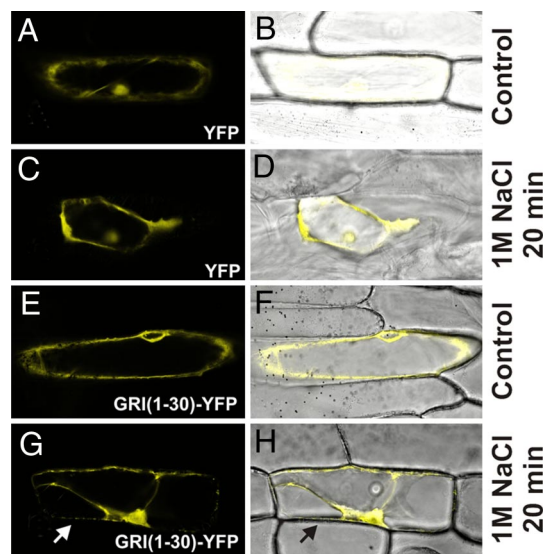
Fig. 4. GRI-signal peptide-YFP localizes to the cytoplasm and extracellular space of transformed onion cells. Onion epidermis was bombarded with DNA-coated gold particles to examine the expression of different constructs. (*A* and *B*) YFP expression in onion epidermis cells, YFP and YFP-transmission light overlay are shown. (*C* and *D*) After plasmolysis with 1 M NaCl for 20 min, the cytoplasm detached from the cell walls. (*E* and *F*) YFP localizes to the nucleus and cytoplasm. GRI-signal peptide-YFP localized in the cytoplasm and perinuclear region of the cells. (*G* and *H*) After plasmolysis the recombinant protein was detectable in the cytoplasm but also remaining in the cell wall where plasma membrane and cytoplasm have detached (arrows).

1B), the incomplete complementation of *gri* by a genomic clone (Fig. 1B), as well as the apparent release of an N-terminal fragment (Fig. 2A), implies a gain-of-function model for the truncated GRI protein. RT-PCR analysis showed that a 5′ part of the *GRI* transcript was still present in *gri* and, thus a truncated GRI protein, similar in size to the fragment that is released from the N terminus of GRI, could be produced. Infiltration of a recombinant peptide corresponding to this truncated protein induced cell death in *Arabidopsis* leaves. This suggests that the GRI N-terminal part is involved in the regulation of cell death. This, however, poses the question of how *gri* plants survive under normal growth conditions in the presence of a potentially lethal truncated GRI protein. Our results point out that GRI-peptide needs an additional signal for the cell death induction. However, it is also possible that *gri* plants, facing the challenge of "living" in the presence of the peptide, might survive through up-regulation of negative regulators of cell death.

ROS are involved in the regulation of various types of cell death (7). Removal of superoxide by coinfiltration of the GRI-peptide with SOD reduced cell death to control levels. A weaker reduction was observed by H_2O_2 removal with catalase. Plant respiratory burst oxidases (*Atrboh*) are proposed to be a major source of extracellular superoxide. *AtrbohD* and *AtrbohF* are the highest expressed members in leaves (13). Interestingly, cell death induced by GRI peptide was eliminated in *atrbohD* (and the double *atrbohD/F*) but not in *atrbohF*. This suggests that superoxide derived from *AtrbohD* is required for GRI peptide-induced cell death. The differential response of *atrbohD* and *atrbohF* is consistent with earlier results showing different functions for these mutants; *atrbohD* lacked most ROS production in response to a fungal pathogen whereas *atrbohF* allowed for enhanced cell death and improved pathogen resistance (13). The role of superoxide in cell death initiation by GRI-peptide is further supported by the increased sensitivity of *gri* to X/XO, as well as the increased resistance to a virulent bacterial pathogen. The superoxide produced upon pathogen infection triggers cell death, which is enhanced by the truncated GRI protein, subsequently leading to pathogen resistance. This makes GRI-peptide a potential candidate for being involved in ROS-induced cell death. This role of the N-terminal GRI-peptide could explain the phenotype of *gri* plants as well as the phenotypes of the GRI overexpression lines and the genomic complementation lines. Developmental cell death has a clear role in plant reproductive biology (18). Given the abundance of ROS in floral organs and their involvement in pollen tube growth (6), the presence of a truncated GRI peptide in *gri* plants offers also an explanation for the reduced seed content in *gri* siliques as preactivated GRI-peptide in the presence of ROS may lead to misregulated developmental cell death.

Infiltration of GRI-peptide into *sid2*, impaired in SA production, abolished the induction of cell death. This suggested that cell death caused by infiltration of GRI-peptide depends on SA. However, O_3 induction of SA accumulation and expression of SA marker genes were reduced in *gri*. This implied that *gri* might be preprimed for the execution of cell death, or have altered sensitivity to SA, and only need a low increase in SA levels to execute the cell death program.

The presence of a signal peptide for the secretory pathway and induction of cell death by infiltration of GRI-peptide into the extracellular space of *Arabidopsis* leaves points to a function of GRI in the extracellular space. This is supported by secretion of STIG1 into the stigmatic lipid exudate (15) and binding of LeSTIG1 to the extracellular domain of RLKs (16). Because of the very weak expression of *GRI* in *Arabidopsis* leaves, analysis of the subcellular localization of GRI required overexpression with the 35S promoter. Microscopic analysis of GRI-YFP localization suggested both cytosolic and extracellular localization for GRI-YFP. Similarly, when fused to YFP [GRI(1–30)-YFP],

the GRI signal peptide directed YFP to the cell wall. Localization of the GRI-YFP fusion protein to the cytoplasm might be due to mislocalization caused by the 35S promoter, or an additional stimulus or protein might be required for correct GRI localization (19). Furthermore, fluorescent proteins frequently become unstable in the extracellular environment, accounting for very low fluorescence levels (19). Further experiments will be required for determining the precise subcellular localization under control and stress conditions using an inducible promoter system and a transgenic approach in *Arabidopsis*. Taken together, our results provide evidence that the GRI protein is secreted to the extracellular space and can perceive signals there.

The O_3-sensitive phenotype of *gri* can serve as a model for ROS regulation of cell death under stress conditions and potentially also during flower development. The *gri* mutant shows a way to short-circuit the cell death regulation leading to increased cell death under conditions of oxidative stress in the extracellular space. Our results suggest that GRI is involved in mediating the effects of extracellular superoxide for the regulation of cell death. The presence of truncated GRI peptide is sufficient for the initiation of ROS-induced cell death. It will be interesting to analyze the mechanisms that regulate this property of GRI protein in the future.

Materials and Methods

Plant Material and Growth Conditions. The dSPM insertion line SM_3.39219 (N125930) was obtained from the Nottingham *Arabidopsis* Stock Centre (http://nasc.nott.ac.uk) together with other insertion lines (listed in Table S1). Presence of the insertion and homozygous plants were verified by PCR using gene-specific primers (SI Text). Stomatal conductance was analyzed as previously described (20). *sid2-1* was obtained from Jean-Pierre Métraux (University of Fribourg, Fribourg, Switzerland), *triple fad* was obtained from John Browse (Washington State University, Pullman, WA), and *atrbohD*, *atrbohF* and *atrbohD/F* were obtained from Miguel Torres (Universidad Politecnica de Madrid, Spain).

Ozone Treatments. Twenty-one-day-old *Arabidopsis* plants were exposed to 300 ppb O_3 for 6 h. Samples were harvested at the indicated times after the onset of the ozone treatment. Cell death was quantified by ion leakage as previously described (21).

Quantitative PCR Analysis. RNA was isolated as described (22). Total RNA (5 μg) was DNaseI-treated (Fermentas) and used for cDNA synthesis with SuperScript III (Invitrogen) and Ribolock RNase Inhibitor (Fermentas) according to manufacturers' instructions. The reaction was diluted to a final volume of 50 μL, and 1 μL of cDNA was used as template for PCR by using LightCycler 480 SYBR green I master (Roche Diagnostics) on a LightCycler 480 (Roche Diagnostics) in triplicate. The raw threshold cycle (Ct) values were normalized to Actin-2 and expression ratios calculated by the $2^{-\Delta\Delta Ct}$ method. Primer sequences are available in SI Text.

Vapor-Phase Hormone Extraction. The plant hormones SA, JA, and ABA were extracted according to an adapted protocol (23). Measurement by gas chromatography (Thermo Finnigan), and quantification was carried out according to manufacturer's instructions.

Superoxide Treatments. Extracellular superoxide [xanthine/xanthine oxidase in sodium phosphate buffer, 10 mM (pH7)] was vacuum infiltrated into completely expanded detached leaves from 5-week-old plants as previously described (21, 22). Cell death was measured at indicated times with a Conductivity Meter (Mettler Toledo). Nitroblue tetrazolium (NBT) staining was carried out as previously described (22).

Genetic Complementation and Generation of *GRI*-c-myc/StrepII-Overexpression Plants. For genetic complementation the *GRI* locus including the promoter and the 3′ untranslated region were amplified by using specific primers (SI Text) and cloned into the binary plant expression vector pGreenII0029 (24). Homozygous single-insertion plants were selected by segregation analysis.

Full-length or truncated versions of the *GRI* cDNA were amplified by using specific primers and sequenced. They were cloned into pGreenII0029 under control of the Cauliflower Mosaic Virus 35S promotor, tagged with c-myc/StrepII or YFP, respectively, and transformed into Col-0 by floral dipping (25).

For the construction of GST-GRI-peptide, the corresponding part of the cDNA was amplified by using specific primers and cloned into the bacterial expression vector pGEX-4T-1 (GE Healthcare Lifesciences) and subsequently sequenced.

Protein Extraction and Western Blot Analysis. Total protein was extracted from leaves by grinding in homogenization buffer (*SI Text*), followed by centrifugation. Protein amounts in the supernatant were determined by the Bio-Rad Protein Assay according to the manufacturer's specifications. For Western blot analysis, equal amounts of proteins were separated by 12% SDS/PAGE and blotted to polyvinylidene difluoride (PVDF) membranes (Bio-Rad). Membranes were probed with α-c-myc antibodies (A-14; Santa-Cruz). Horseradish peroxidase-conjugated goat anti-rabbit IgG (Sigma) was used as a secondary antibody. The reaction was detected by enhanced chemoluminescence by using the Supersignal Pico detection kit (Thermo Scientific).

Peptide Infiltration. GST-GRI-peptide was produced in *E. coli* BL21-RIL Codon plus cells (Stratagene) and purified by using Glutathione Sepharose 4B (GE Healthcare Lifesciences) according to manufacturer's instructions. The GST-tag was removed by using thrombin (GE Healthcare Lifesciences) according to manufacturer's instructions. Proteins were quantified by using the Bio-Rad Protein Assay.

GRI-peptide, with or without CAT (Roche) or SOD (Sigma), was diluted to a final concentration of 100 ng/mL in 10 mM sodium phosphate buffer (pH7) and infiltrated into fully expanded leaves of 5-week-old plants. Four leaf disks were cut out, rinsed, and pooled in 5 mL of MilliQ water. Ion leakage was measured by using a conductivity meter.

P. syringae Growth Curve Assay. *P. syringae pv*. tomato DC3000 (*Pst*) or *Pst* DC3000 avrRpt2+ was used in all experiments (26). Bacteria were grown on NYG medium (0.5% trypton peptone; 0.3% yeast extract; 2% glycerol) plus 1.5% bacto-agar at 28 °C. For plant infection, liquid cultures were inoculated from plates and grown in NYG medium at 28 °C overnight. Plants were vacuum-infiltrated, and bacterial growth was assessed as described (26). Ion leakage was measured as described above.

Onion Transformation by Particle Bombardment. DNA-coated gold particles (0.6 μm; Bio-Rad) were prepared according to manufacturer's instructions. Onion epidermal cells were transformed via bombardment with a Helios Gene Gun (Bio-Rad) according to manufacturer's instructions. After transformation, the epidermis was floated on 20 mL of 0.5× MS medium in the dark overnight. YFP expression was analyzed with a Leica TCS SP5 confocal microscope. Plasmolysis was carried out after overnight incubation immediately before microscopic analysis by immersing the epidermal peels in 0.5× MS medium with 1 M NaCl for 20 min as previously described (3).

Phylogenetic and Statistical Analysis. Sequence alignments were performed by using the Clustal W program (27). Neighbor-joining trees and matrices were constructed by using the Mega 4 software package (28). One hundred boot-strap sets were used.

1. Kangasjärvi J, Jaspers P, Kollist H (2005) Signalling and cell death in ozone-exposed plants. *Plant Cell Environ* 28:1021–1036.
2. Valko M, et al. (2007) Free radicals and antioxidants in normal physiological functions and human disease. *Int J Biochem Cell Biol* 39:44–84.
3. Vahisalu T, et al. (2008) SLAC1 is required for plant guard cell S-type anion channel function in stomatal signalling. *Nature* 452:487–491.
4. Carol RJ, Dolan L (2006) The role of reactive oxygen species in cell growth: Lessons from root hairs. *J Exp Bot* 57:1829–1834.
5. McInnis SM, Desikan R, Hancock JT, Hiscock SJ (2006) Production of reactive oxygen species and reactive nitrogen species by angiosperm stigmas and pollen: Potential signalling crosstalk? *New Phytol* 172:221–228.
6. Potocky M, et al. (2007) Reactive oxygen species produced by NADPH oxidase are involved in pollen tube growth. *New Phytol* 174:742–751.
7. Overmyer K, Brosche M, Kangasjärvi J (2003) Reactive oxygen species and hormonal control of cell death. *Trends Plants Sci* 8:335–342.
8. Miller G, Mittler R (2006) Could heat shock transcription factors function as hydrogen peroxide sensors in plants? *Ann Bot* 98:279–288.
9. Despres C, et al. (2003) The *Arabidopsis* NPR1 disease resistance protein is a novel cofactor that confers redox regulation of DNA binding activity to the basic domain/leucine zipper transcription factor TGA1. *Plant Cell* 15:2181–2191.
10. Davletova S, et al. (2005) Cytosolic ascorbate peroxidase 1 is a central component of the reactive oxygen gene network of *Arabidopsis. Plant Cell* 17:268–281.
11. Bozhkov PV, Filonova LH, Suarez MF (2005) Programmed cell death in plant embryogenesis. *Curr Top Dev Biol* 67:135–179.
12. Jabs T, Dietrich RA, Dangl JL (1996) Initiation of runaway cell death in an *Arabidopsis* mutant by extracellular superoxide. *Science* 273:1853–1856.
13. Torres MA, Dangl JL, Jones JD (2002) *Arabidopsis* gp91^{phox} homologues *AtrbohD* and *AtrbohF* are required for accumulation of reactive oxygen intermediates in the plant defense response. *Proc Natl Acad Sci USA* 99:517–522.
14. Goldman MH, Goldberg RB, Mariani C (1994) Female sterile tobacco plants are produced by stigma-specific cell ablation. *EMBO J* 13:2976–2984.
15. Verhoeven T, et al. (2005) STIG1 controls exudate secretion in the pistil of petunia and tobacco. *Plant Physiol* 138:153–160.
16. Tang W, Kelley D, Ezcurra I, Cotter R, McCormick S (2004) LeSTIG1, an extracellular binding partner for the pollen receptor kinases LePRK1 and LePRK2, promotes pollen tube growth in vitro. *Plant J* 39:343–353.
17. Overmyer K, et al. (2008) Complex phenotypic profiles leading to ozone sensitivity in *Arabidopsis thaliana* mutants. *Plant Cell Environ* 31:1237–1249.
18. Wu HM, Cheung AY (2000) Programmed cell death in plant reproduction. *Plant Mol Biol* 44:267–281.
19. Berg RH, Beachy RN (2008) Fluorescent protein applications in plants. *Methods Cell Biol* 85:153–177.
20. Kollist T, et al. (2007) A novel device detects a rapid ozone-induced transient stomatal closure in intact Arabidopsis and its absence in abi2 mutant. *Physiol Plant* 129:796–803.
21. Overmyer K, et al. (2000) Ozone-sensitive *Arabidopsis* rcd1 mutant reveals opposite roles for ethylene and jasmonate signaling pathways in regulation superoxide-dependent cell death. *Plant Cell* 12:1849–1862.
22. Overmyer K, et al. (2005) Ozone-induced programmed cell death in the *Arabidopsis radical-induced cell death1* mutant. *Plant Physiol* 137:1092–1104.
23. Schmelz EA, et al. (2003) Simultaneous analysis of phytohormones, phytotoxins, and volatile organic compounds in plants. *Proc Natl Acad Sci USA* 100:10552–10557.
24. Hellens RP, et al. (2000) pGreen: A versatile and flexible binary Ti vector for *Agrobacterium*-mediated plant transformation. *Plant Mol Biol* 42:819–832.
25. Clough SJ, Bent AF (1998) Floral dip: A simplified method for *Agrobacterium*-mediated transformation of *Arabidopsis thaliana. Plant J* 16:735–743.
26. Yu IC, Parker J, Bent AF (1998) Gene-for-gene disease resistance without the hypersensitive response in *Arabidopsis dnd1* mutant. *Proc Natl Acad Sci USA* 95:7819–7824.
27. Larkin MA, et al. (2007) Clustal W and clustal X version 2.0. *Bioinformatics* 23:2947–2948.
28. Tamura K, Dudley J, Nei M, Kumar S (2007) MEGA4: Molecular Evolutionary Genetics Analysis (MEGA) software version 4.0. *Mol Biol Evol* 24:1596–1599.